

Squeezing Flow of Viscoplastic Fluids Subject to Wall Slip

ADENIYI LAWAL*

*Department of Chemical Engineering
King Fahd University of Petroleum & Minerals
Dhahran 31261, Saudi Arabia*

and

DILHAN M. KALYON

*Highly Filled Materials Institute
Chemistry and Chemical Engineering Department
Stevens Institute of Technology
Castle Point, Hoboken, New Jersey 07030*

Polymer processing operations such as compression molding, sheet forming and injection molding can be modeled by squeezing flows between two approaching parallel surfaces in relative motion. Squeezing flows also find applications in the modeling of lubrication systems, and in the determination of rheological properties. Here, analytical solutions are developed for the constant-speed squeezing flow of viscoplastic fluids. It is assumed that the fluid is purely viscous, and hence viscoelastic effects unimportant. The rheological behavior of the viscoplastic fluids is represented by the Herschel-Bulkley viscosity function. The deformation behavior of commonly encountered viscoplastic fluids is generally complicated by the presence of wall slip at solid walls, which is a function of the wall shear stress. The slip coefficient that relates the slip velocity to the shear stress is affected by the material of construction and also the roughness of the solid surfaces, leading to the possibility of different slip coefficients at various solid surfaces. The model developed in this study accommodates the use of different slip coefficients at different solid surfaces. The accuracy of the solutions is established, and the effects of various parameters such as slip coefficient and apparent yield stress are examined. The solutions provide useful design expressions that can be utilized for squeezing flows of viscoplastic fluids, with or without wall slip at the solid boundaries.

INTRODUCTION

The generally highly viscous nature of polymeric materials plays a prominent role in the selection of a suitable processing operation, as well as processing conditions. For instance, certain polymeric materials having very high viscosity (e.g. ultra-high molecular weight polyethylene) are more readily processed by positive displacement techniques such as compression molding (1), a processing operation that can be modeled as a squeezing flow of fluid between two solid surfaces. Squeezing flows are also encountered in other polymer processing operations such as sheet

forming and injection molding (2). An accurate and reliable prediction of the generated flow pattern is essential in such operations since the flow pattern impacts greatly on the material properties of the finished product. For example, in the compression molding of fiber-reinforced composites, the flow patterns determine not only the fiber orientation, but also the curing behavior of the processed material. Another area of practical importance where squeezing flows find relevance is in the modeling of lubrication systems (e.g. the meshing of a gear teeth), where extremely large pressures are developed under unsteady state conditions when a fluid is confined in a small clearance between two solid surfaces that approach each other in relative motion.

Squeezing flows are characterized by both shearing

*To whom correspondence should be addressed.

and biaxial extensional deformations under transient conditions. Close to the solid walls, the flow is dominated by shear, but in the region near the center plane, the flow is primarily extensional. By assuming that the squeezing flow of a material is describable by a particular hydrodynamic problem, squeezing flows have been used for the determination of material functions such as shear and biaxial elongational viscosities, and stress relaxation of highly viscous materials. The materials that have been used include polymer melts (1, 3, 4), and elastomers (5, 6). Rheological constitutive equations can also be tested using this procedure. For the reasons outlined, the study of squeezing flows is not only of theoretical interest but also of practical significance.

A large number of polymeric materials, including gels and concentrated suspensions (7–10), and melts of commodity resins such as polyethylenes (11–14), and polyvinylchloride (15) have been observed to exhibit wall slip at solid surfaces. Various mechanisms have been proposed for wall slip at the liquid-solid interface region. In flows of concentrated suspensions, the apparent slip mechanism is related to the migration of particles away from the wall, which creates a thin low viscosity fluid layer next to the wall and a core of highly viscous fluid. With such large viscosity gradients within the flow, the thin low viscosity fluid thus appears to slip past the solid surface because of its negligible resistance to flow. With gels and concentrated suspensions, the apparent wall slip mechanism may dominate the flow behavior (9, 10) for a wide range of wall shear stress values as there exists a strong interplay between the wall slip and the fluid mechanics at the liquid-solid boundary. In compression molding of polymeric composites, large viscosity gradients are believed to arise from large temperature differences that usually exist between the walls of the mold and the processed material. The high temperature, low viscosity material that is formed next to the wall essentially acts like a lubricant, creating an apparent slip, i.e. a relative velocity between the material and the wall (16, 17).

In squeezing flows, with the no-slip condition at the walls, the flow in the region close to the walls is shear dominated, and the velocity distribution assumes the usual parabolic form for fluids that do not exhibit viscoplasticity. If, on the other hand, a perfect slip is imposed at the walls, the flow will be primarily extensional and consequently, the velocity profile will be of the plug flow type. Neither of these two conditions correctly characterizes the flow. A finite non-zero wall slip coefficient will best represent the interfacial constitutive equation, and the capability to handle such boundary conditions renders the analysis contained in this article especially relevant, as most studies, with the exception of the work reported by Zhang *et al.* (18), are applicable only to the no-slip wall condition. In addition, most investigations, both theoretical and experimental, have been restricted to fluids that do not exhibit viscoplasticity, a rheological behavior

that is commonly observed in gels and concentrated suspensions.

In the following, we present analytical and exact solutions for the velocity distributions as well as the force, in squeezing flows of viscoplastic fluids with wall slip. The elastic deformation is neglected and the fluid is assumed to be describable by the Herschel-Bulkley viscosity function thus permitting various simplifications such as the Bingham plastic, the power law fluid of Ostwald-de Waele, and the Newtonian fluid.

ANALYSIS

The viscoplastic fluid is contained in the gap formed by two horizontal parallel circular disks that are of the same radius, R , and are both initially at rest (Fig. 1). The fluid subsequently undergoes squeezing action by either applying a constant force F to the top disk or by moving it at a constant speed \dot{h} , with the bottom disk remaining at rest. If the applied force is constant, the speed of the top disk will vary with time, and vice-versa. Therefore, the flow is time-dependent. However, the flow is dominated by viscous effects, thus permitting the treatment of the flow as quasi-static, i.e. the flow is steady at any instant of time, and the time derivatives of the equations of conservation of mass and momentum can be ignored. Since the thickness of the fluid, h , is usually much smaller than the radius of the disk ($h \ll R$), it is conventional to model the flow using the lubrication approximation that essentially allows the neglect of the inertia force in the equation of motion. If gravitational effects are also neglected, the flow in essence becomes one-dimensional, and is radial in the cylindrical coordinate system considered here.

According to the argument presented by Lipscomb and Denn (19), squeeze film flow of a Herschel-Bulkley material cannot contain a yield surface as previous analytical solutions (20) using lubrication theory suggest. One attempt at the resolution of this inconsistency involves the modification of the Herschel-Bulkley model. One such model is the bi-viscosity model, (21, 22), which essentially introduces an

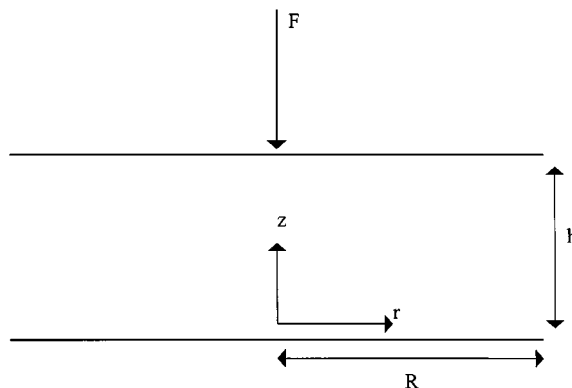


Fig. 1. Schematic of the model of squeezing flow between two parallel disks with the top disk moving with speed \dot{h} while the bottom disk remains stationary.

additional parameter to describe the rheological behavior of viscoplastic materials at low shear rates. Although the application of lubrication theory to the squeezing flow of viscoplastic fluids using the Herschel-Bulkley rheological model leads to kinematic inconsistency, squeeze film measurements (23, 24) carried out on a model Herschel-Bulkley fluid suggest that the analytical solution based on the lubrication theory provides a useful first approximation.

Following the lubrication approximation, the equation of continuity and the r -component of the equation of motion are given respectively by:

$$\frac{1}{r} \frac{\partial}{\partial r} r v_r + \frac{d v_z}{d z} = 0 \quad (1a)$$

$$\frac{\partial}{\partial z} \tau_{rz} = -\frac{d p}{d r} \quad (1b)$$

where r is the radial coordinate, p is the pressure, and τ_{rz} is the shear stress. To obtain a solution to Eqs 1, a constitutive model need be specified. Here the fluid is assumed to be a purely viscous generalized Newtonian fluid that is characterized rheologically by the Herschel-Bulkley viscosity function. Applying again the lubrication approximation, the model equations are:

$$\tau_{rz} = -m \left| \frac{\partial v_r}{\partial z} \right|^{n-1} \frac{\partial v_r}{\partial z} \pm \tau_o \quad |\tau_{rz}| \geq \tau_o \quad (2a)$$

$$\frac{\partial v_r}{\partial z} = 0 \quad |\tau_{rz}| \leq \tau_o \quad (2b)$$

Here, m and n are material parameters and τ_o is the yield stress, i.e. a critical value of the stress magnitude below which viscoplastic materials do not deform. The minus sign is to be used when $\tau_{rz} < 0$. At stress magnitudes $|\tau_{rz}|$ that are less than the yield stress, only the rigid body motion, i.e. plug flow is possible.

Defining the following dimensionless variables:

$$v_r^* = v_r / (-\dot{h}); \quad r^* = r/R; \quad z^* = z/R; \quad \frac{d p^*}{d r^*} = R \left(\frac{d p}{d r} \right) / m \left(\frac{-\dot{h}}{R} \right)^n \quad (3a)$$

where \dot{h} is the speed of the top disk, Eq 1b becomes

$$\frac{\partial}{\partial z^*} \left(\left| \frac{\partial v_r^*}{\partial z^*} \right|^{n-1} \frac{\partial v_r^*}{\partial z^*} \right) = \frac{d p^*}{d r^*} \quad (3b)$$

Equation 3b is applicable only in the deformation region and is replaced by the rigid body translation requirement, Eq 2b, in the plug region whenever it exists. The boundary conditions to Eq 3b are provided by the Navier's slip at the wall condition, which is of the form (25).

$$\underline{t} \cdot (\underline{v} - \underline{v}_{solid}) = \beta (\underline{n} \cdot \underline{t} : \underline{\pi}) \quad (4)$$

where \underline{t} is the unit tangent vector to the surface n is the unit outward normal, and β is the slip parameter.

In general, β may depend on the invariants of the stress tensor, but here it is assumed to be a material constant which for a given fluid depends on the material of construction and roughness of the solid surfaces.

If we apply Eq 4 to the geometry under consideration, we have:

$$v_r^{*sb} = -\beta_b \tau_{rz}(0) / (-\dot{h}) \quad (5a)$$

$$v_r^{*st} = -\beta_t \tau_{rz}(h) / (-\dot{h}) \quad (5b)$$

where v_r^{*st} and v_r^{*sb} are the dimensionless radial velocity of the fluid at the top and bottom disks, respectively, β_t and β_b are the corresponding slip parameters, and $\tau_{rz}(0)$ and $\tau_{rz}(h)$ are related through:

$$\tau_{rz}(h) = h \left(\frac{-d p}{d r} \right) + \tau_{rz}(0) \quad (6)$$

The results of numerical experimentation revealed that there are four distinct flow regimes (Fig. 2) that are described by the solutions to Eq 3 depending on the values of the parameters of the problem. The solutions to these different cases can be expressed more compactly in terms of the following dimensionless parameters:

$$\alpha_1 = \left(\frac{\beta_b m}{-\dot{h}} \right) \left(\frac{-\dot{h}}{R} \right)^n \quad (7a)$$

$$\alpha_2 = \left(\frac{\beta_t m}{-\dot{h}} \right) \left(\frac{-\dot{h}}{R} \right)^n \quad (7b)$$

$$\kappa_1 = \left(\frac{\beta_b \tau_o}{-\dot{h}} \right) \quad (7c)$$

$$\kappa_2 = \left(\frac{\beta_t \tau_o}{-\dot{h}} \right) \quad (7d)$$

$$h^* = h/R \quad (7e)$$

$$s = 1/n \quad (7f)$$

The four cases are:

- Case 1: Plug region attached to the top disk ($\beta_t \neq 0$, Fig. 2a)

$$v_r^* = \left(\frac{-d p^*}{d r^*} \right)^s \frac{\lambda_1^{s+1}}{(s+1)} - \left(\frac{-d p^*}{d r^*} \right)^s \frac{(\lambda_1 - z^*)^{s+1}}{(s+1)} + \kappa_1 + \alpha_1 \left(\frac{-d p^*}{d r^*} \right) \lambda_1 \quad 0 \leq z^* \leq \lambda_1 \quad (8a)$$

$$v_r^* = \left(\frac{-d p^*}{d r^*} \right)^s \frac{\lambda_1^{s+1}}{(s+1)} + \kappa_1 + \alpha_1 \left(\frac{-d p^*}{d r^*} \right) \lambda_1 \quad \lambda_1 \leq z^* \leq h^* \quad (8b)$$

The parameter λ_1 , which designates the lower interface between the deformation region and the plug flow region is governed by the equation:

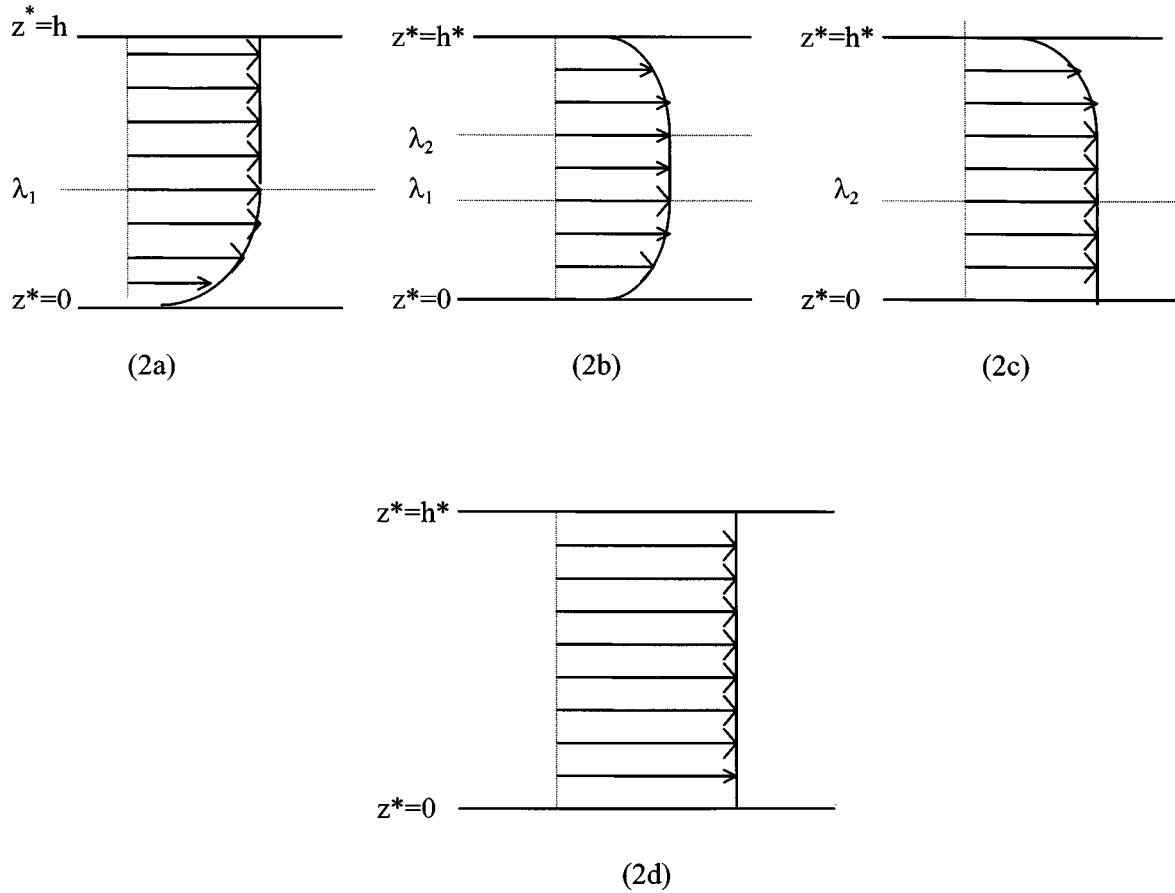


Fig. 2. Schematic representation of the radial velocity profiles for the four possible cases.

$$\left(\frac{-dp^*}{dr^*}\right)^s \frac{\lambda_1^{s+1}}{(s+1)} + \left(\frac{-dp^*}{dr^*}\right) \lambda_1 (\alpha_1 + \alpha_2) - \alpha_2 h^* \left(\frac{-dp^*}{dr^*}\right) + \kappa_1 + \kappa_2 = 0 \quad (8c)$$

while the equation for the pressure gradient is obtained by integrating the continuity equation (Eq 1a), and is given by:

$$\left(\frac{-dp^*}{dr^*}\right)^s \frac{\lambda_1^{s+1}}{(s+1)} h^* - \left(\frac{-dp^*}{dr^*}\right)^s \frac{\lambda_1^{s+2}}{(s+1)(s+2)} + \alpha_1 h^* \lambda_1 \left(\frac{-dp^*}{dr^*}\right) + \kappa_1 h^* - \frac{r^*}{2} = 0 \quad (8d)$$

Equations 8c and 8d are solved simultaneously to obtain the values of λ_1 and dp^*/dr^* at any radial location r^* for given values of the flow parameters.

- Case 2: Floating plug region (Fig. 2b)

$$v_r^* = \left(\frac{-dp^*}{dr^*}\right)^s \frac{\lambda_1^{s+1}}{(s+1)} - \left(\frac{-dp^*}{dr^*}\right)^s \frac{(\lambda_1 - z^*)^{s+1}}{(s+1)} + \kappa_1 + \alpha_1 \left(\frac{-dp^*}{dr^*}\right) \lambda_1 \quad 0 \leq z^* \leq \lambda_1 \quad (9a)$$

$$v_r^* = \left(\frac{-dp^*}{dr^*}\right)^s \frac{(h^* - \lambda_2)^{s+1}}{(s+1)} + \alpha_2 h^* \left(\frac{-dp^*}{dr^*}\right) - \kappa_2 - \alpha_2 \left(\frac{-dp^*}{dr^*}\right) \lambda_1 \quad \lambda_1 \leq z^* \leq \lambda_2 \quad (9b)$$

$$v_r^* = \left(\frac{-dp^*}{dr^*}\right)^s \frac{(h^* - \lambda_2)^{s+1}}{(s+1)} - \left(\frac{-dp^*}{dr^*}\right)^s \frac{(z^* - \lambda_2)^{s+1}}{(s+1)} + \alpha_2 h^* \left(\frac{-dp^*}{dr^*}\right) - \kappa_2 - \alpha_2 \left(\frac{-dp^*}{dr^*}\right) \lambda_1 \quad \lambda_2 \leq z^* \leq h^* \quad (9c)$$

The equation for λ_1 is given by:

$$\left(\frac{-dp^*}{dr^*}\right)^s \left[h^* - \lambda_1 - \frac{2\tau_o}{m \left(\frac{-h}{R}\right)^n \left(\frac{-dp^*}{dr^*}\right)} \right]^{s+1} - \alpha_2 \left(\frac{-dp^*}{dr^*}\right) (\lambda_1 - h^*) - \alpha_1 \left(\frac{-dp^*}{dr^*}\right) \lambda_1 - \kappa_1 - \kappa_2 - \left(\frac{-dp^*}{dr^*}\right)^s \frac{\lambda_1^{s+1}}{(s+1)} = 0 \quad (9d)$$

and λ_2 , the upper interface between the deformation region and the plug flow region is subsequently obtained from:

$$\lambda_2 = \lambda_1 + \frac{2\tau_o}{m\left(\frac{-\dot{h}}{R}\right)^n \left(\frac{-dp^*}{dr^*}\right)} \quad (9e)$$

The pressure gradient is related to λ_1 , and λ_2 through the following equation:

$$\left(\frac{-dp^*}{dr^*}\right)^s \frac{h^*(h^* - \lambda_2)^{s+1}}{(s+1)} - \frac{\left(\frac{-dp^*}{dr^*}\right)^s}{(s+1)(s+2)}$$

$$[(h^* - \lambda_2)^{s+2} + \lambda_1^{s+2}] - \kappa_2 h^* - \alpha_2 h^* \left(\frac{-dp^*}{dr^*}\right)$$

$$(\lambda_1 - h^*) - \frac{r^*}{2} = 0 \quad (9f)$$

• Case 3: Plug region attached to bottom disk ($\beta_b \neq 0$, Fig. 2c)

$$v_r^* = \left(\frac{-dp^*}{dr^*}\right)^s \frac{(h^* - \lambda_2)^{s+1}}{(s+1)} + \alpha_2 h^* \left(\frac{-dp^*}{dr^*}\right)$$

$$- \alpha_2 \left(\frac{-dp^*}{dr^*}\right) \lambda_2 + \kappa_2 \quad 0 \leq z^* \leq \lambda_2 \quad (10a)$$

$$v_r^* = \left(\frac{-dp^*}{dr^*}\right)^s \frac{(h^* - \lambda_2)^{s+1}}{(s+1)} - \left(\frac{-dp^*}{dr^*}\right)^s$$

$$\frac{(z^* - \lambda_2)^{s+1}}{(s+1)} + \alpha_2 h^* \left(\frac{-dp^*}{dr^*}\right) - \alpha_2 \left(\frac{-dp^*}{dr^*}\right)$$

$$\lambda_2 + \kappa_2 \quad \lambda_2 \leq z^* \leq h^* \quad (10b)$$

The parameter λ_2 is governed by the following equation:

$$\left(\frac{-dp^*}{dr^*}\right)^s \frac{(h^* - \lambda_2)^{s+1}}{(s+1)} - (\alpha_2 + \alpha_1) \left(\frac{-dp^*}{dr^*}\right) \lambda_2$$

$$+ \alpha_2 h^* \left(\frac{-dp^*}{dr^*}\right) + \kappa_2 + \kappa_1 = 0 \quad (10c)$$

while the pressure gradient is related to λ_2 through the following equation:

$$\left(\frac{-dp^*}{dr^*}\right)^s \frac{(h^* - \lambda_2)^{s+1}}{(s+1)} h^* - \left(\frac{-dp^*}{dr^*}\right)^s$$

$$\frac{(h^* - \lambda_2)^{s+2}}{(s+1)(s+2)} - \alpha_2 \left(\frac{-dp^*}{dr^*}\right) h^* \lambda_2 + \alpha_2 h^{*2}$$

$$\left(\frac{-dp^*}{dr^*}\right) + \kappa_2 h^* - \frac{r^*}{2} = 0 \quad (10d)$$

Equations 10c and 10d need be solved simultaneously to obtain λ_2 and dp^*/dr^* .

• Case 4: Plug flow throughout the flow domain ($\beta_t \neq 0$, $\beta_b \neq 0$, Fig. 2d)

Since the flow in this case is due to slip, neither the top disk slip parameter nor the bottom disk slip parameter can be zero; however, their values can be different. The fluid velocity for this flow regime is obtainable from:

$$v_r^* = \frac{\alpha_1 h^* \left(\frac{dp^*}{dr^*}\right)}{(1 + \beta_b/\beta_t)} \quad (11a)$$

with the pressure gradient given by:

$$\frac{-dp^*}{dr^*} = \frac{r^*}{2\alpha_1 h^{*2}} (1 + \beta_b/\beta_t) \quad (11b)$$

Both Eqs 11a and 11b can also be written in terms of the top disk parameter α_2 .

Determination of Force F

The z-component of the surface traction vector (assuming compressive stresses positive) is:

$$\pi_{zz} = p + \tau_{zz} \quad (12a)$$

and the total force needed to maintain the squeezing flow is obtained by integrating this traction over the surface of the top disk.

Hence,

$$F = \int_0^{2\pi} \int_0^R ((p - p_\alpha) + \tau_{zz})_{z=h} r dr d\theta \quad (12b)$$

where p_α is the pressure at the edge of the disk, and the stress component τ_{zz} for the Herschel-Bulkley fluid is given by:

$$\tau_{zz} = -2 \left(m |\dot{\gamma}|^{n+1} + \frac{\tau_o}{|\dot{\gamma}|} \right) \frac{\partial v_z}{\partial z} \quad (12c)$$

Following the lubrication approximation, $\frac{\partial v_z}{\partial z}$ is negligible, therefore:

$$F = 2\pi \int_0^R (p - p_\alpha)_{z=h} r dr \quad (12d)$$

After carrying out the necessary integration, and introducing the dimensionless variables, the dimensionless total force $F^* = F/mR^2 (-\dot{h}/R)^n$ is given by:

$$F^* = \pi \int_0^1 (r^*)^2 \left(\frac{-dp^*}{dr^*}\right) dr^* \quad (12e)$$

RESULTS AND DISCUSSION

For a given set of rheological and geometrical parameters, as well as the operating conditions, the appropriate case among the four possible velocity profiles was selected, and the nonlinear equations for the values of the extremum locations λ_1 , λ_2 , and the dimensionless pressure gradient dp^*/dr^* were solved using the Newton-Raphson technique with a general relative tolerance of 10^{-6} . The velocity profiles and the dimensionless total force were next obtained from the relevant equations. The analytical solutions were verified by comparing our results with well-known results

available in the literature. For several selected values of rheological and geometrical parameters, the total force values obtained from our analytical solutions were compared with those from Stefan (26) for a Newtonian fluid and Scott (27) for a power-law fluid. The agreement was excellent, and the relative differences were less than 0.1% for all the cases selected for comparison. The analytical solutions were next compared with the experimental force data in (18) on constant-speed squeezing of polymer melts for the case where there is no slip. As shown in Figs. 3a and b for high-density polyethylene and linear low-density polyethylene respectively, the agreement between the analytical predictions and the experimental data is very good, and the slight differences are within expected experimental error.

The effects of various parameters such as the slip coefficient, and the yield stress on the velocity, pressure gradient, and the applied force distributions will be examined in a number of case studies using realistic values of parameters and operating conditions. The values are as indicated in Table 1 and the parametric variations will be indicated in the figures. However, before these case studies are discussed, representative velocity profiles that will help elucidate the results

Table 1. The Geometry, Operating Conditions, and Material Parameters Used in the Case Studies.

Material Parameters	
Herschel-Bulkley fluid	
Shear-rate sensitivity parameter n	$0.25 \leq n \leq 1.25$
$m = 6888 \text{ Pa}\cdot\text{s}^n$	
Apparent yield stress τ_o	$20 \leq \tau_o \leq 10,000 \text{ Pa}$
Navier's wall slip coefficient β	$0 \leq \beta \leq 7.2 \times 10^{-8} \text{ m/Pa}\cdot\text{s}$
Disk Geometry and Operating Conditions	
Gap h	$= 2.5 \times 10^{-3} \text{ m}$
Disk radius R	$= 28.6 \times 10^{-3} \text{ m}$
Top disk speed	$= 8.5 \times 10^{-6} \text{ m/s}$

of the case studies must be presented. In all the results to be presented here, and subsequently, the squeezing flow is assumed to be generated by moving the top disk at a constant speed with a force that is allowed to vary with time, while the bottom disk remains stationary.

The axial distributions of dimensional radial velocity profiles at selected radial coordinates are shown in Figs. 4a-c. For finite non-zero values of slip coefficients at the top and bottom disk surfaces, and an apparent yield stress, the velocity profile at the edge of the disks

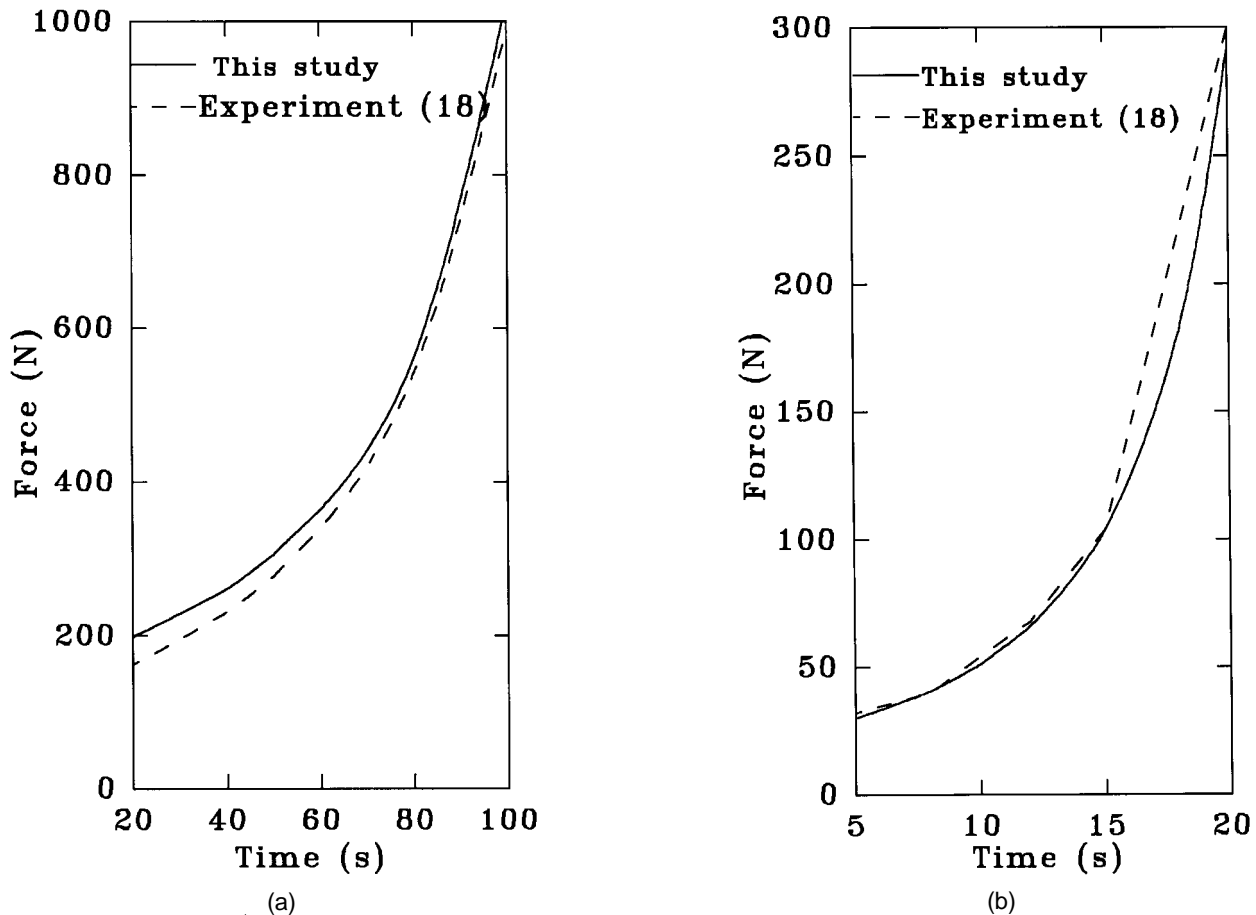


Fig. 3. Comparison of model predictions of force with experimental force measurements for constant-speed squeezing of: (a) HDPE with $m = 4.49 \times 10^4 \text{ Pa}\cdot\text{s}^{0.25}$ and $n = 0.25$ (18); (b) LLDPE with $m = 5.91 \times 10^3 \text{ Pa}\cdot\text{s}^{0.6}$ and $n = 0.6$ (18) without wall slip.

is Case 2 type, i.e., the plug region is sandwiched between the top and bottom disks. Along the axis of the disks, i.e. at a radial coordinate of zero, the shear stress is zero everywhere and hence the radial velocity. The radial velocity profile therefore, must go through a transition from the Case 2 profile at the outer edge of the disk to the Case 4 profile along the axis of the disks. The transition velocity profile is determined by the relative values of the slip coefficients at the bottom and top disks surfaces. As we proceed from the outer edge towards the axis of the disks, the value of λ_2 increases while that of λ_1 decreases, hence the thickness of the plug flow region (i.e. $\lambda_2 - \lambda_1$) increases as more of the fluid is at a shear stress value less than that of the yield stress. The relative movement of the λ_1 and λ_2 values depends on the relative values of the top and bottom disks slip coefficients, and thus determines whether the transition velocity profile will be that of Case 1, Case 3 or Case 4 velocity profile.

In Fig. 4a, the slip coefficient at the surface of the top disk is lower than that at the bottom disk surface, and the λ_1 location therefore moves more rapidly than the λ_2 location. Consequently, the transition velocity profile is Case 3 with the plug region attached to the bottom surface. When the slip coefficient at the surface of the top disk (β_t) is higher than that of the bottom disk surface (β_b), a reverse behavior is obtained with a transition radial velocity profile of Case 1 (plug region attached to the top disk surface). If both the top and bottom disk slip coefficients are the same, the λ_1 and λ_2 locations move at the same rate, hence the velocity profile goes from Case 2 to Case 4 (i.e. plug flow throughout) without any transition velocity profile (Fig. 4b).

(a) Effect of the Shear-Rate Sensitivity Parameter n

The parameter n governs the sensitivity of the material to deformation rate and its effect on the radial velocity v_r profiles is shown in Fig. 5a when the no-slip boundary condition is imposed at the disks surfaces and other parameters are as indicated in Table 1. In the region close to the disks surfaces, and for a fixed axial coordinate, z , the flow is shear dominated, and as the parameter n increases, the velocity decreases and so does the velocity gradient. Since the same mass flow rate is imposed, in order to satisfy the mass-conservation constraint, with increased n we would expect that the decrease in fluid velocity in the wall regions will be compensated for by an increase in fluid velocity as the center region is approached giving rise to a cross-over behavior. The pressure gradient, and the total force profiles can now be examined in the light of the velocity profiles of Figs. 4 and 5a. For any value of the parameter n , as we proceed from the center of the disks to the outer edge, generally, the shear stress τ_{rz} increases, and the requirement of momentum conservation in the radial direction implies a corresponding increase in the pressure gradient as observable in Fig. 5b. Also, at any radial coordinate r , as n increases the pressure gradient decreases on account of decreased velocity gradient which results in decreased shear stress τ_{rz} .

The development of the total force profile as the disks approach each other is shown in Fig. 5c for varying parameter n . As the disk spacing is decreased or correspondingly as time increases, at constant-speed squeezing, the total force applied to the moving

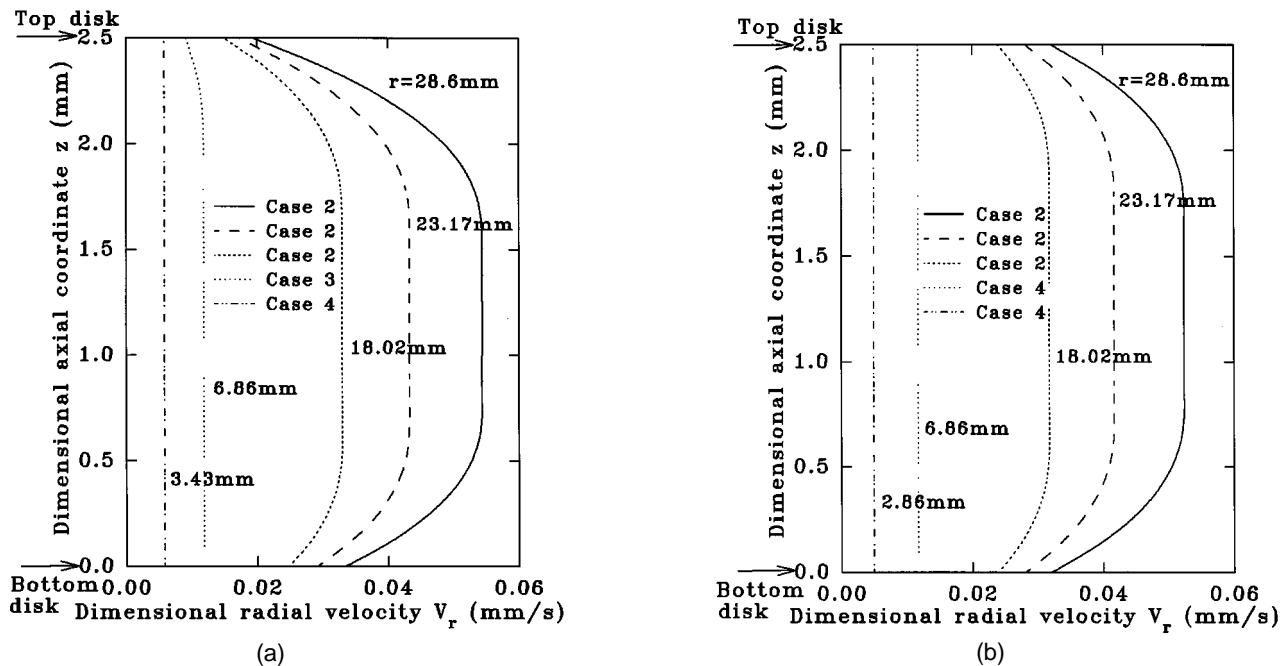


Fig. 4. Typical dimensional radial velocity profiles for squeezing flow of viscoplastic fluids with $n = 0.75$, $\tau_0 = 500 \text{ Pa}$, $m = 6888 \text{ Pa}\cdot\text{s}^{0.75}$ and (a) $\beta_t = 1.2 \times 10^{-8} \text{ m/Pa}\cdot\text{s}$, $\beta_b = 2.4 \times 10^{-8} \text{ m/Pa}\cdot\text{s}$; (b) $\beta_t = \beta_b = 2.4 \times 10^{-8} \text{ m/Pa}\cdot\text{s}$.

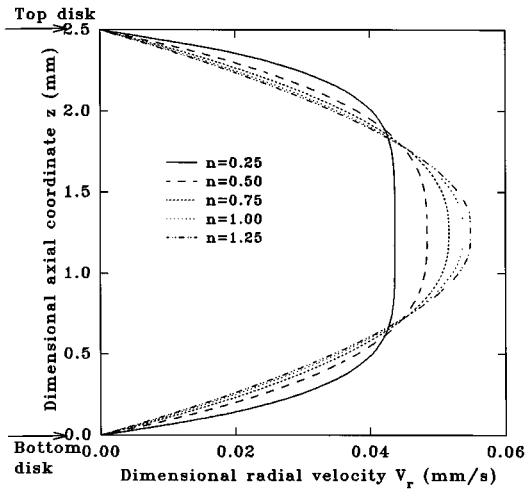


Fig. 5a. Dimensional radial velocity profiles in constant-speed squeezing flow with $\tau_0 = 20 \text{ Pa}$, $\beta_t = \beta_b = 0.0$ and varying shear-rate sensitivity parameter n .

top disk increases for any value of n as would be expected from the lubrication approximation theory. The pressure gradient increases with decreased n as observed in Fig. 5b, and with negligible normal stress, the total force is accounted for by the pressure gradient. The total force therefore increases with decreased n at any disk spacing h .

(b) Effect of the Slip Coefficient β

In considering the effect of the slip coefficient on the velocity, pressure gradient, and total force profiles, it is expedient to set the slip coefficients at both disks surfaces equal, i.e. $\beta_b = \beta_t = \beta$. If $\beta = 0$, which corresponds to the no-slip condition, the velocity of the fluid at the disk surfaces will be the same as that of the disks surfaces, which in this case is zero. However, on imposing a non-zero β value, the fluid velocity at the disks surfaces attains a non-zero and positive value, which increases as β increases (Fig. 6a). Since the mass flow rate is kept constant, as we vary the slip coefficient β , the increase in the fluid velocity in the disk surfaces region will result in decreased veloc-

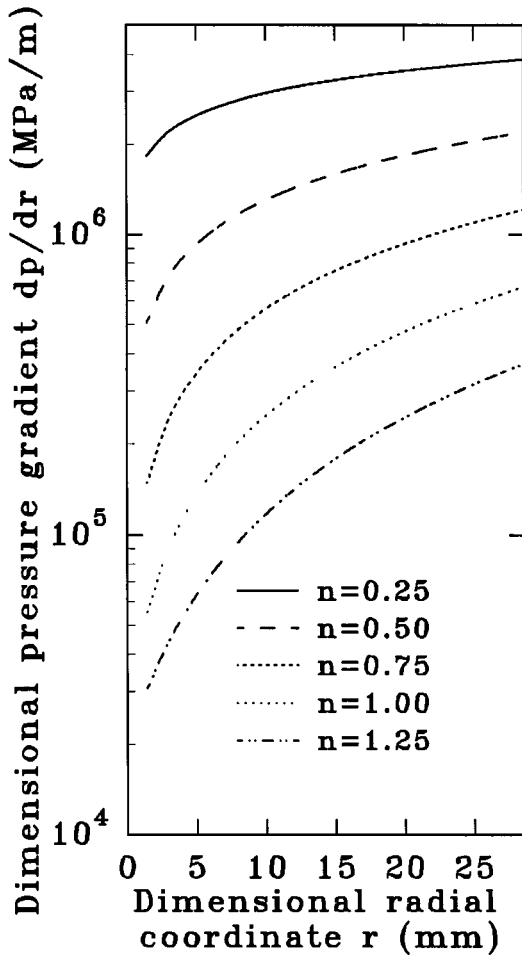


Fig. 5b. Dimensional pressure gradient profiles in constant-speed squeezing flow with $\tau_0 = 20 \text{ Pa}$, $\beta_t = \beta_b = 0.0$ and varying shear-rate sensitivity parameter n .

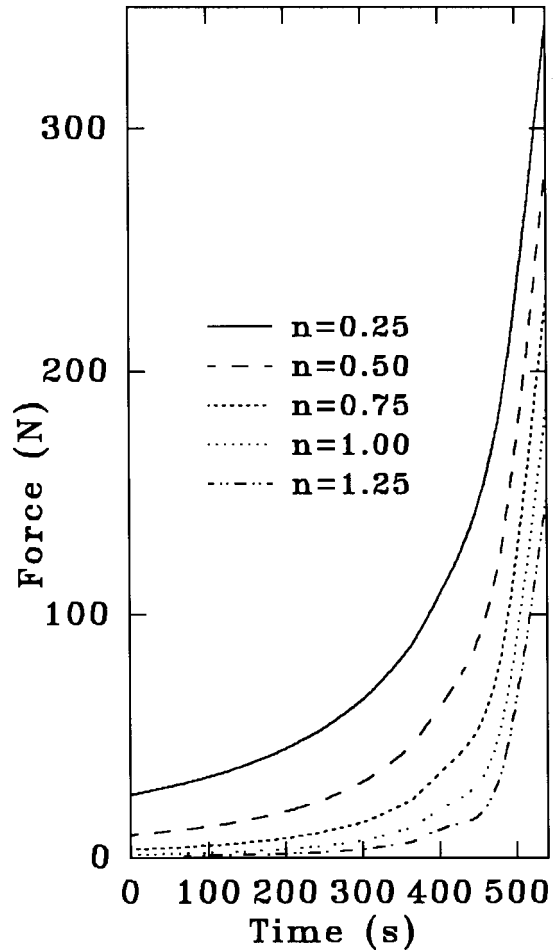


Fig. 5c. Dimensional force profiles in constant-speed squeezing flow with $\tau_0 = 20 \text{ Pa}$, $\beta_t = \beta_b = 0.0$ and varying shear-rate sensitivity parameter n .

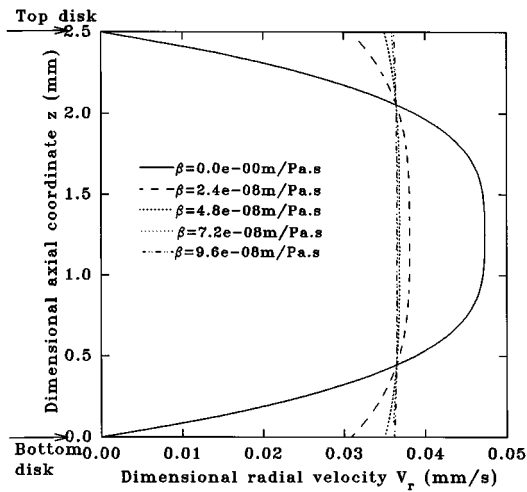


Fig. 6a. Dimensional radial velocity profiles in constant-speed squeezing flow with $\tau_0 = 20 \text{ Pa}$, $n = 0.43$ and varying slip coefficient $\beta_t = \beta_b = \beta$.

ity gradients there, and in the center region the fluid will be correspondingly slowed down as β is increased, otherwise the mass conservation requirement will be violated. This is clearly observable in Fig. 6a where at high values of β , the velocity profile greatly departs from the usual parabolic form and is replaced by the almost plug flow velocity profile that typifies extensional flows.

A reduction in velocity gradient will necessarily give rise to decreased shear stress, hence as indicated in Fig. 6b, the pressure gradient sharply decreases with increased β at any radial coordinate. On the basis of this observation, the total force required to maintain the constant-speed squeezing flow should similarly be affected by the existence of wall slip, and as shown in Fig. 6c, for fluids that exhibit significant wall slip, a far smaller total force is required in comparison to a fluid with zero slip coefficient. In addition, the total force grows less rapidly as the disk spacing 'h' is decreased for fluids with high β values and in fact at early times, the growth is almost imperceptible.

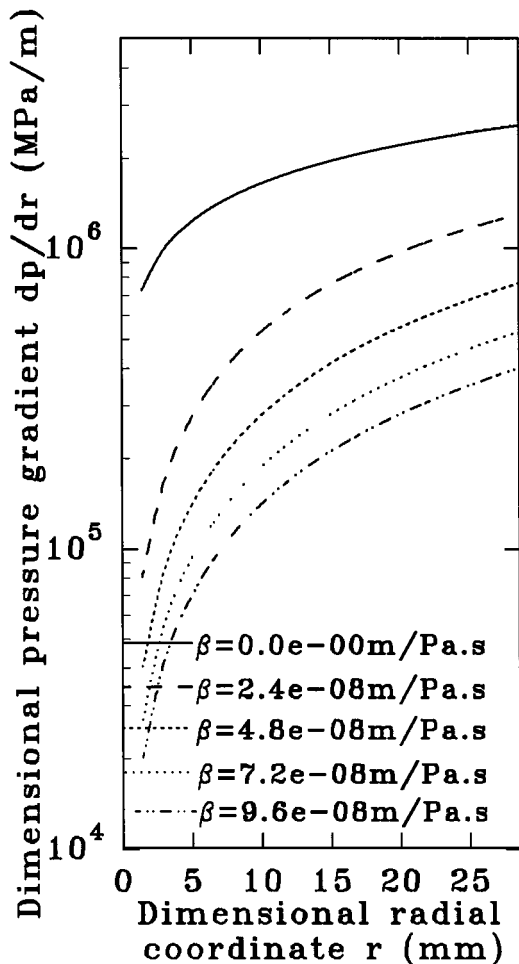


Fig. 6b. Dimensional pressure gradient profiles in constant-speed squeezing flow with $\tau_0 = 20 \text{ Pa}$, $n = 0.43$ and varying slip coefficient $\beta_t = \beta_b = \beta$.

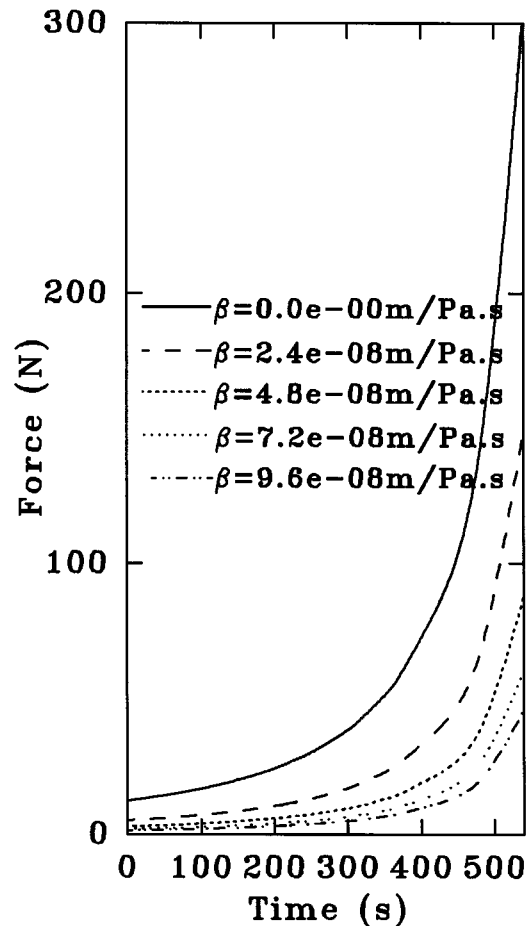


Fig. 6c. Dimensional force profiles in constant-speed squeezing flow with $\tau_0 = 20 \text{ Pa}$, $n = 0.43$ and varying slip coefficient $\beta_t = \beta_b = \beta$.

(c) Effect of the Ratio $\beta_t/\beta_b(\phi)$

In situations where the materials of construction or the roughness profiles of the top and bottom disks surfaces are different, the slip coefficients at the two surfaces would be different, therefore a capability for incorporating different slip coefficients in the analysis of squeezing flow is of importance. In examining the effect of the ratio $\phi(\beta_t/\beta_b)$, the value of the slip coefficient at the bottom disk surface will be fixed at 9.6×10^{-8} m/Pa.s while β_t will be varied. The velocity profile at the top disk surface can be seen to be significantly affected by ϕ . As ϕ is changed from zero (Fig. 7a), the velocity of the fluid next to the top disk surface experiences a steep increase, and thereafter the effect is attenuated. The velocity of the fluid in the region close to the bottom disk is similarly affected, although to a lesser extent. Since the fluid velocity at the top disk surface increases as ϕ is increased, a reverse behavior is expected at the bottom disk surface for the mass conservation requirement to be satisfied. The overall effect, in essence, is the reduction of the velocity gradient and the rendering of the velocity profile plug like. The effect of ϕ on both the pressure gradient and the total force is therefore predictably, a decrease with increased ϕ in the light of the velocity profiles. This is qualitatively similar to the effect of β . These results, taken together, could provide a means of achieving optimum processing or operating conditions for fluids that exhibit wall slip by proper engineering of surfaces either in terms of material selection or the intentional roughening of surfaces to create the desired ϕ value.

(d) Effect of the Yield Stress τ_o

The flow profiles of fluids that exhibit viscoplasticity are greatly influenced by the magnitude of the yield

stress τ_o . Any region subjected to a stress magnitude less than the yield stress will not experience any deformation, and when such regions are continuous, they produce plug flow structures. The stress distribution within the flow domain dictates the extent and location of the plug region. In constant-speed squeezing flow, in the absence of wall slip behavior, the stress magnitude is minimum midway between the top and bottom disk surfaces, and the plug region is therefore centered here (Fig. 8a). When $\tau_o = 0$, i.e. no yield stress, the velocity profile is parabolic. As τ_o increases, steep velocity gradients develop in the regions of the disk surfaces while in the center the velocity of the fluid reduces in compensation, and the size of the plug region increases.

The effect of τ_o on the dimensional pressure gradient is shown in Fig. 8b, where for a fixed radial coordinate, as τ_o increases, the pressure gradient also increases. In addition, for fluids with yield stress, the change in the pressure gradient is abrupt in a very small region close to the axis of the disks and away from this region, the pressure gradient is more or less constant. Increased pressure gradient with increased τ_o should expectedly give rise to increased total force

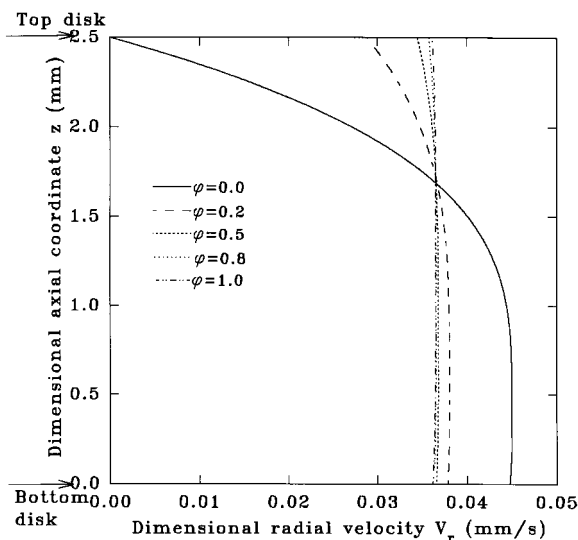


Fig. 7a. Dimensional radial velocity profiles in constant-speed squeezing flow with $\tau_o = 20$ Pa, $n = 0.43$ and varying ϕ .

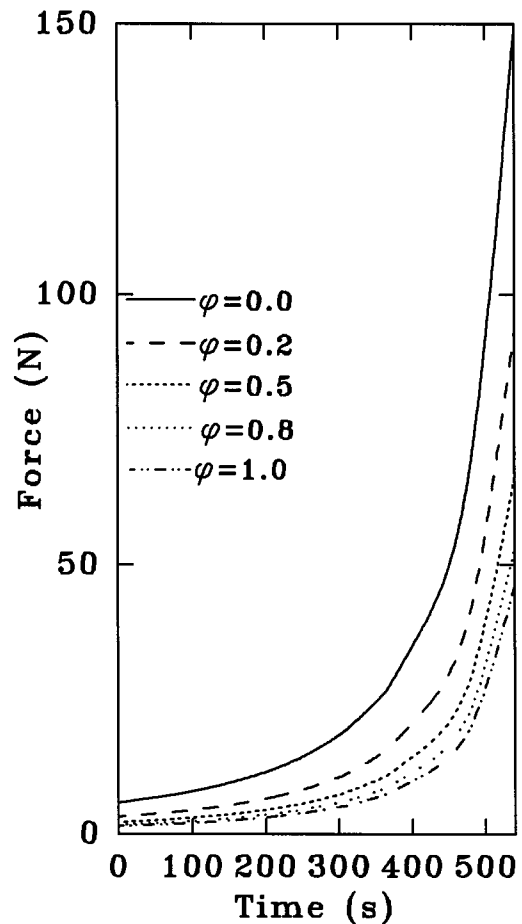


Fig. 7b. Dimensional force profiles in constant-speed squeezing flow with $\tau_o = 20$ Pa, $n = 0.43$ and varying ϕ .

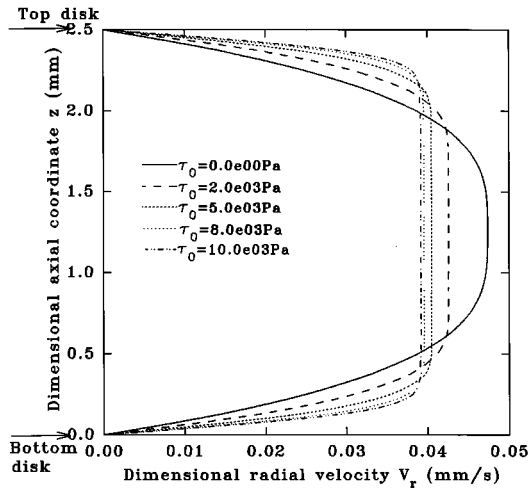


Fig. 8a. Dimensional radial velocity profiles in constant-speed squeezing flow with $n = 0.43$, $\beta_t = \beta_b = 0.0$ and varying apparent yield stress τ_0 .

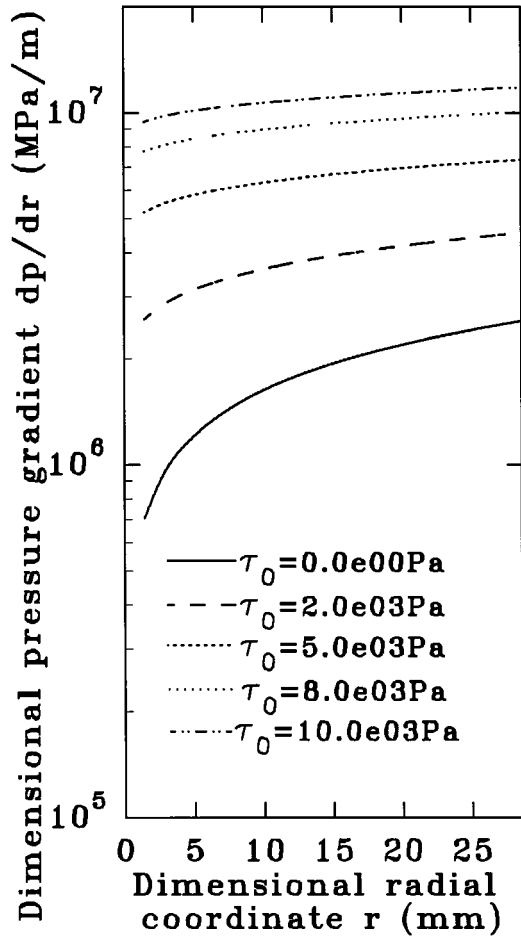


Fig. 8b. Dimensional pressure gradient profiles in constant-speed squeezing flow with $n=0.43$, $\beta_t = \beta_b = 0.0$ and varying apparent yield stress τ_0 .

as confirmed by the results of Fig. 8c. The effect of τ_0 on both the pressure gradient and the total force is related to the increase in shear viscosity of the fluid. As the yield stress increases, the fluid becomes more solid-like and increased values of pressure gradient and total force are required. Even though reduced velocity gradients in the region centered midway between the top and bottom disks when considered alone would imply a reverse outcome, the effect of τ_0 on the shear viscosity appears to be the more dominant for the conditions considered here.

CONCLUSIONS

We have developed general analytical and exact solutions for constant-speed squeezing flows of viscoplastic fluids subject to different slip coefficients at the top and bottom disk surfaces. The accuracy of the solutions has been established by comparisons with literature data, both theoretical and experimental. Since the solutions are analytical, they are applicable over a wide range of parameters, and they provide useful design expressions for processing operations that can be modeled as squeezing flows between two approaching parallel disks.

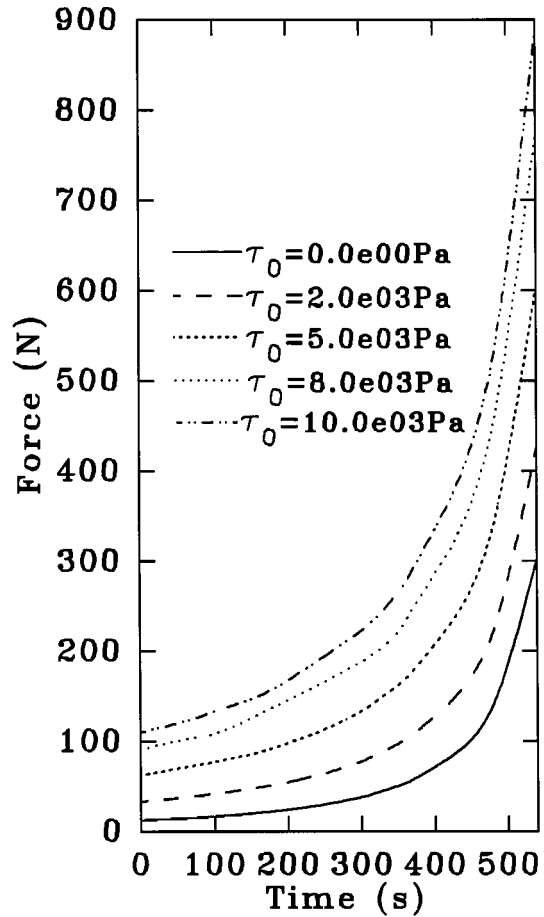


Fig. 8c. Dimensional force profiles in constant-speed squeezing flow with $n = 0.43$, $\beta_t = \beta_b = 0.0$ and varying apparent yield stress τ_0 .

The solutions have been used in assessing the importance of various parameters such as n , the shear-rate sensitivity parameter, the slip coefficient β , the ratio of the top disk slip coefficient to the bottom disk slip coefficient ϕ , and the apparent yield stress τ_o on velocity profile, pressure gradient, and total force required for the squeezing action. An increase in the parameter n results in decreased pressure gradient at any radial coordinate, and consequently a reduction in the total force. The effect of the slip coefficient β or the ratio ϕ is a significant reduction in the velocity gradient everywhere with the velocity profiles transformed from the usual parabolic form, (obtained in shear dominated flow), to plug flow, which typifies extensional flows. Both the pressure gradient and the total force are reduced by increased β , and ϕ . Visco-plasticity produces an opposite effect. Even though the velocity gradient in the region centered midway between the top and bottom disks is reduced by increased τ_o , which would imply a decrease in both the pressure gradient and the total force, the shear viscosity of the fluid is concomitantly increased and appears to be the more dominant effect, thus leading to increased pressure gradient and total force.

ACKNOWLEDGMENT

A. L. would like to express his gratitude to KFUPM for making available some of the computing facilities required for the completion of the work reported here. The typing of the manuscript was excellently done by Mr. E. Esteban.

REFERENCES

1. M. T. Shaw, *Polym. Eng. Sci.*, **17**, 266 (1977).
2. P. J. Leider and R. B. Bird, *Ind. Eng. Chem. Fundam.*, **13**, 336 (1974).
3. P. R. Soskey and H. H. Winter, *J. Rheol.*, **29**, 493 (1985).
4. T. C. Hsu and I. R. Harrison, *Polym. Eng. Sci.*, **31**, 223 (1991).
5. S. H. Chatraei, C. W. Macosko, and H. H. Winter, *J. Rheol.*, **25**, 433 (1981).
6. G. Winther, K. Almdal, and O. Kramer, *J. Non-Newtonian Fluid Mech.*, **39**, 119 (1991).
7. T. Q. Jiang, A. C. Young, and A. B. Matzner, *Rheol. Acta* **25**, 397 (1986).
8. E. Windhab and W. Gleissle, *Proc. 9th Intl. Congress on Rheology*, Mexico (1984).
9. U. Yilmazer and D. M. Kalyon, *J. Rheol.*, **33**, 1197 (1989).
10. D. M. Kalyon, U. Yilmazer, P. Yaras, and B. Aral, *J. Rheol.*, **37**, 35 (1993).
11. L. L. Blyer, Jr. and A. C. Hart, Jr. *Polym. Eng. Sci.*, **10**, 193 (1970).
12. A. V. Ramamurthy, *Adv. Polym. Technol.*, **6**(4), 489 (1986).
13. S. G. Hatzikiriakos and J. M. Dealy, *J. Rheol.*, **35**, 497 (1991).
14. Y. Chen, D. M. Kalyon, and E. Bayramli, *J. Appl. Polym. Sci.*, **50**, 1169 (1993).
15. A. V. Ramamurthy, *J. Rheol.*, **30**, 337 (1986).
16. M. R. Barone and D. A. Caulk, *Polym. Compos.*, **6**, 105 (1985).
17. W. Michaeli, M. Mahlke, and T. A. Osswald, *Kunststoffe*, **80**, 30 (1990).
18. W. Zhang, N. Silvi, and J. Vlachopoulos, *Intern. Polym. Processing*, **10**, 155 (1995).
19. G. G. Lipscomb and M. M. Denn, *J. Non-Newtonian Fluid Mech.*, **14**, 337 (1984).
20. G. H. Covey and B. R. Stanmore, *J. Non-Newtonian Fluid Mech.*, **8**, 249 (1981).
21. D. K. Gartling and N. Phan-Tien, *J. Non-Newtonian Fluid Mech.*, **14**, 347 (1984).
22. S. D. R. Wilson, *J. Non-Newtonian Fluid Mech.*, **47**, 211 (1993).
23. M. J. Adams, B. Edmonson, D. G. Caughey, and R. Yahya, *J. Non-Newtonian Fluid Mech.*, **51**, 61 (1994).
24. M. J. Adams, B. J. Briscoe, and M. Kamjab, *Adv. Colloid Interface Sci.*, **44**, 143 (1993).
25. A. Lawal and D. M. Kalyon, *Polym. Eng. Sci.*, **34**, 1471 (1994).
26. J. Stefan and K. Sitzgber, *Akad. Wiss. Math. Natur. Wien*, **69**, 713 (1874).
27. J. R. Scott, *Trans. Inst. Rubber Ind.*, **7**, 169 (1931).

Received July 8, 1997
Revised December 1997